Two-Dimensional Hexagonal Mesoporous Silica Thin Films Prepared from Block Copolymers: Detailed Characterization and Formation Mechanism

ARTICLE *in* CHEMISTRY OF MATERIALS · APRIL 2001

Impact Factor: 8.35 · DOI: 10.1021/cm001225b

6 AUTHORS, INCLUDING:

David Grosso
Collège de France
207 PUBLICATIONS **8,652** CITATIONS
SEE PROFILE

Heinz Amenitsch
Graz University of Technology
375 PUBLICATIONS **8,335** CITATIONS
SEE PROFILE

Florence Babonneau
Pierre and Marie Curie University - Paris 6
314 PUBLICATIONS **9,041** CITATIONS
SEE PROFILE

Two-Dimensional Hexagonal Mesoporous Silica Thin Films Prepared from Block Copolymers: Detailed Characterization and Formation Mechanism

D. Grosso,*,† A. R. Balkenende,‡ P. A. Albouy,§ A. Ayral,|| H. Amenitsch,⊥ and F. Babonneau†

Laboratoire Chimie de la Matière Condensée, Université Pierre et Marie Curie, 4 Place Jussieu, 75252 Paris Cedex 05, France, Philips Research Laboratories, Prof. Holstlaan 4, 5656 AA Eindhoven, Netherlands, Laboratoire de Physique des Solides, Université Paris-Sud, 91405 Orsay Cedex, France, Laboratoire des Matériaux et Procédés Membranaires, UMR 5635, CNRS, ENSCM, UMII, 8 rue de l'Ecole Normale, 34296 Montpellier Cedex 5, France, and Institute of Biophysics and X-ray Structure Research, Austrian Academy of Sciences, Steyrergasse 17/VI, 8010 Graz, Austria

Received November 17, 2000

Silica thin films with a two-dimensional (2D) hexagonal structure were produced from TEOS and the F127 triblock copolymer $PEO_{106}PPO_{70}PEO_{106}$. The structure of the films was deduced from transmission electron microscopy (TEM) performed on microtomed sections and from a 2D X-ray scattering technique adapted for film characterization. Both methods are complementary and allow for a detailed characterization of the film structure. The pore channels within the coatings are organized in domains, which spin and curve inside the film, but align with the surface plan at the air/film and film/substrate interfaces. The formation of the film was monitored by in situ time-resolved SAXS experiments to follow the structural evolution during the first minutes after deposition. Cylindrical micelles, which gives rise to a wormlike structure, form first at the air/film interface and extend toward the film/substrate interface via solvent evaporation. When most of the liquid phase is evaporated, the well-aligned domains located at both interfaces are obtained by a self-arrangement of the micelles parallel to the interfaces. This rearrangement occurs when the film is considered to be dry. The atom content profiles in the as-prepared films were obtained by Rutherford backscattering (RBS) and show homogeneous distribution of atoms throughout the film thickness. To stiffen the network and remove the surfactant, various postsynthesis treatments were applied to the coatings, that is, thermal treatment, base-catalyzed condensation, and solvent extraction. Each method induces shrinkage, leading to 2D-centered rectangular films through a contraction of the initial 2D hexagonal structure. As-prepared and treated films exhibit excellent optical transparency and high degree of organization. Ellipsometry measurements and N_2 adsorption/desorption isotherms were thus used to estimate the refractive index and the porosity of the films. Refractive index down to 1.2 was obtained in the film that was pretreated under a NH_3 atmosphere before solvent extraction of the surfactant. This shows the efficiency of this treatment to minimize the network shrinkage. N_2 adsorption−desorption measurement performed on films calcined at 350 °C gives a surface area of 800 $m^2\ g^{-1}$ and a porosity of 63%.

1. Introduction

Since the discovery of the MCM-type mesoporous materials,[1,2] an increasing interest has been shown in the design of novel porous materials tailored with various pore organization and dimensions for potential applications in separation, catalysis, encapsulation, chemical sensing, and low-dielectric and optical coatings. The synthesis process of mesoporous materials involves the formation of organic−inorganic composites by a self-assembly process, where the organic phase is organized on a mesoscopic scale, and serves as a template for the inorganic skeleton.[3−5] One can obtain

* To whom correspondence should be addressed. E-mail: grosso@ccr.jussieu.fr.
† Université Pierre et Marie Curie.
‡ Philips Research Laboratories.
§ Université Paris-Sud.
|| ENSCM, UMII.
⊥ Austrian Academy of Sciences.

(1) Vartuli, J. C.; Schmitt, K. D.; Kresge, C. T.; Roth, W. J.; McCullen, S. B.; Hellring, S. D.; Beck, J. S.; Schlenker, J. L.; Olson, D. H.; Sheppard, E. W. *Chem. Mater.* **1994**, *6*, 2317.
(2) Beck, J. S.; Vartuli, J. C.; Roth, W. J.; Leonovicz, M. E.; Kresge, C. T. Schmidt, K. D.; Chu, C. T.−W.; Olson, D. H.; Sheppard, E. W.; McCullen, S. B.; Higgins, J. B.; Schlenker, J. L. *J. Am. Chem. Soc.* **1992**, *114*, 10834.
(3) Barton, T. J.; Bull, L. M.; Klemperer, W. G.; Loy, D. A.; McEnaney, B.;. Misono, M.; Monson, P. A.; Pez, G.; Scherer, G. W.; Vartuli, J. C.; Yaghi, O. M. *Chem. Mater.* **1999**, *11*, 2633.
(4) Ciesla, U.; Schuth, F. *Microporous Macroporous Mater.* **1999**, *27*, 131.
(5) Ying, J. Y.; Mehnert, C. P.; Wong, M. S. *Angew. Chem., Int. Ed.* **1999**, *38*, 56.

10.1021/cm001225b CCC: $20.00
Published on Web 04/28/2001

different mesostructures and pore sizes by adjusting the synthesis conditions and the surfactant nature. Silica materials, exhibiting lamellar, 2D hexagonal (*p*6*m*), 3D hexagonal ($P6_3/mmc$), or cubic (*Ia*3*d*, *Im*3*m*, and *Pm*3*n*) organizations, with the pore size ranging from 15 to 40 Å, have been produced with ionic surfactants such as alkyltrimethylammonium bromide or chloride, or double-headed gemini quaternary ammonium salts, with various alkyl chain lengths.[1,6−9] Mesoporous materials, synthesized with nonionic poly(ethylene oxide)−polypropylene oxide−poly(ethylene oxide) block copolymer surfactants (Pluronics, $PEO_x-PPO_y-PEO_x$), have recently been shown to have high degrees of organization, high porosity, and large pore diameters (20−300 Å).[10] The use of these block copolymers to obtain ordered inorganic porous matrixes is one of the most promising routes in terms of high porosity, large-pore dimension, high degree of ordering, low cost, and low toxicity.

For a large range of applications such as antireflective coatings, low dielectric constant layers, optical sensors, or membranes, it would be desirable to produce such mesoporous materials in the form of thin films.

Silica nanostructured materials, produced with block copolymer surfactants, have already been studied in the various forms of bulks,[10,11] films,[12] and fibers.[13] Zhao et al. have reported the formation of 2D hexagonal films with Pluronic P123 ($PEO_{20}-PPO_{70}-PEO_{20}$) and cubic films with Pluronic F127 ($PEO_{106}-PPO_{70}-PEO_{106}$).[12] Films are usually prepared by liquid deposition methods such as spin coating, dip coating, or epitaxial growth.[14,15] For spin and dip coating, the sols are diluted and the concentrations in reagents are fixed as to prevent fast condensation of the inorganic precursors. Indeed, chemistry should be turned off to enable the organization of the amphiphilic molecules to occur. Ethanol is chosen as the solvent for its good wettability properties with glass or silicon substrates. During deposition by dip coating, a layer of solution is dragged onto the substrate surface. The alcohol and then the water depart from the air/film interface, inducing the concentrations in inorganic precursor, acid, and surfactant to increase gradually. Therefore, the formation of mesoporous films is somehow different than the formation of powdered materials as the experimental conditions are in constant evolution. The mesostructure of the film forms via evaporation-induced self-assembly[16] for which the solvent evaporation simultaneously induces the formation of micelles, their self-assembly with the oligomeric inorganic species, and the polycondensation of the network. This implies that the organization, condensation, and drying of the films occur in the few minutes following the substrate withdrawal from the sol. There is thus a strong need to use in situ characterization techniques to get some insights in real time into the film formation mechanism. There are few attempts in that direction in the literature: spatially resolved fluorescence-depolarization experiments were performed to identify micelle formation during film deposition.[6] More recently, in situ luminescence of probe molecules was used to follow the chemical and structural changes occurring during the formation of lamellar films.[17] All these optical techniques, even if extremely useful, do not provide any information on the organization of the film and its related geometry.

As a result of the large difference between thickness and surface dimensions, and of the interactions existing at the film/substrate interface, coatings generally undergo a contraction in the direction normal to the surface during drying and aging. Additional shrinkage leading to an overall decrease in pore volume can be induced by various treatments applied to stiffen the network and remove the organic templates from the pores. Ideally, it is desirable to keep the highest possible degree of organization in the films after treatment, while still retaining the highest porosity and the initial pore dimension. However, as a result of the conditions used, the silica network of as-deposited films is far from being highly condensed,[16] and one can thus expect the inorganic network structures to be easily affected by postdeposition treatments that will favor condensation reactions and, thus, network strengthening. Heat treatment at $T = 400$ °C is generally accompanied by a large shrinkage of the structure.[18] Moreover, such mesoporous coatings may be applied to certain devices that may not accept such treatment. We have therefore investigated low-temperature treatments, which involve two steps. The first step implies the soft condensation of the inorganic skeleton by reaction with an NH_3 atmosphere or heat treatment at a moderate temperature (160 °C) while the surfactant template remains within the pores. Contrary to the calcination at higher temperature (350 °C) for which the template removal and the network condensation occur simultaneously, the presence of the surfactant phase within the pores during the first step allows the contraction of the network to be minimized. The organic phase is then removed in the second step by solvent extraction. In these two-step methods the lattice unidirectional contraction is shown to be lower than that with the one-step calcination technique.

The objective of this paper was to characterize the structural evolution of templated silica thin films prepared with the Pluronic F127 block copolymer, following the various preparation steps based on dip coating, drying, and surfactant removal. The films were produced by dip coating on thin silicon wafers and glass plates. Initial sols were prepared in acidic conditions,

(6) Lu, Y.; Ganguli, R.; Drewien, C. A.; Anderson, M. T.; Brinker, C. J.; Gong, W.; Guo, Y.; Soyez, H.; Dunn, B.; Huang, M. H.; Zink, J. I. *Nature* **1997**, *389*, 364.
(7) Zhao, D.; Yang, P.; Margolese, D. I.; Chmelka, B. F.; Stucky, G. D. *Chem. Commun.* **1998**, 2499.
(8) Ogawa, M.; Ishikawa, H.; Kikuchi, T. *J. Mater. Chem.* **1998**, *8*, 1783.
(9) Tolbert, S. H.; Shaffer, T. E.; Feng, J.; Hansman, P. K.; Stucky, G. D. *Chem. Mater.* **1997**, *9*, 1962.
(10) Zhao, D.; Huo, Q.; Feng, J.; Chmelka, B. F.; Stucky, G. D. *J. Am. Chem. Soc.* **1998**, *120*, 6024.
(11) Melosh, N. A.; Lipic, P.; Bates, F. S.; Wudl, F.; Stucky, G. D.; Fredrickson, G. H.; Chmelka, B. F. *Macromolecules* **1999**, *32*, 4332.
(12) Zhao, D.; Yang, P.; Melosh, N.; Chmelka, B. F.; Stucky, G. D. *Adv. Mater.* **1998**, *10*, 1380.
(13) Yang, P.; Zhao, D.; Chmelka, B. F.; Stucky, G. D. *Chem. Mater.* **1998**, *10*, 2033.
(14) Yang, H.; Kuperman, A.; Coombs, N.; Mamiche-Afara, S.; Ozin, G. A. *Nature* **1996**, *379*, 703.
(15) Yang, G. A.; Coombs, N.; Sokolov, I.; Ozin, G. A. *Nature* **1996**, *381*, 589.
(16) Brinker, C. J.; Lu, Y.; Sellinger, A.; Fan, H. *Adv. Mater.* **1999**, *11*, 579.
(17) Huang, M. H.; Dunn, B. S.; Zink, J. I. *J. Am. Chem. Soc.* **2000**, *122*, 3739.
(18) Kundu, D.; Zhou, H. S.; Honma, I. *J. Mater. Sci. Lett.* **1998**, *17*, 2089.

using tetraethoxysilane (TEOS) as the silica precursor and the Pluronic F127 block copolymer ($OH(CH_2-CH_2O)_{106}(CHCH_3CH_2O)_{70}(CH_2CH_2O)_{106}H$) as the nonionic structuring agent. The structure of the films was investigated by X-ray diffraction (XRD) in transmission and reflection geometries ($\theta-2\theta$ scanning) as well as by transmission electronic microscopy (TEM) performed on microtomed sections. As-prepared films have a 2D hexagonal structure ($p6m$). In situ time-resolved SAXS experiments were performed for the first time on such systems to obtain some insight into the film formation. To do so, 2D X-ray diffraction patterns were recorded on a CCD camera every second after film deposition. The uniaxial shrinkage of the films after surfactant removal was studied by XRD. The atom contents and profiles within the coatings were deduced from Rutherford backscattering (RBS). The porous films were analyzed by variable angle spectroscopic ellipsometry (VASE) and N_2-adsorption/desorption investigation. Films exhibit excellent optical qualities, large domains with high degree of organization, good stability toward treatments, and high surface area and porosity.

2. Experimental Section

2.1. Film Preparation. Pluronic F127 (i.e., $OH(CH_2-CH_2O)_{106}(CHCH_3CH_2O)_{70}(CH_2CH_2O)_{106}H$) was obtained from BASF and used as received. TEOS was obtained from Aldrich and EtOH and HCl from Prolabo. Sols used for deposition were synthesized using the following preparation. A stock solution of prehydrolyzed silica precursor was prepared by refluxing a mixture of 40 g of TEOS, 26.7 g of EtOH, and 3.5 g of H_2O containing 2.7×10^{-3} M HCl for 1 h. It corresponds to the following molar ratios: TEOS:EtOH:H_2O:F127 1:3:1:x. To 7 g of this prehydrolyzed solution, a second solution containing 15.2 g of EtOH, 1.4 g of H_2O (0.055 M HCl), and between 0.5 and 1.5 g (2.1−6.1 wt %) of Pluronic F127 were added. The final sols, which correspond to TEOS:EtOH:H_2O:HCl:F127 1:20:5:0.004:x molar ratios, were stirred for 24 h and aged for 6 days at room temperature in a closed vessel before deposition. Thin films were produced by dip coating at a constant withdrawal rate of 2.5 mm s^{-1}, on glass plates and silicon substrates (8-μm-thick (100) silicon wafers purchased from Virginia Semiconductor, Inc). Substrates were cleaned in 2 M HNO_3 for 12 h at room temperature and successively rinsed with water, ethanol, and acetone to promote the formation of homogeneous coating and good adhesion. After deposition, as-prepared films (labeled S_0) were dried in air for a few hours before undergoing subsequent treatments. The one-step thermal treatment leading to samples labeled S_{350} consisted of heating the samples from 160 to 350 °C in air (ramp of 1 °C min^{-1}) followed by 5 h at 350 °C. The other treatments involved two steps. First, the stiffening of the silica network was done either by base-catalyzed condensation (samples were left in a saturated NH_3 atmosphere for 45 min) or by preheating (samples were left for 1 h at 160 °C in air). Then, the removal of the copolymer was done by Soxhlet extraction in acetone (4−8 h). These samples are labeled S_{NH3}Ac and S_{160}Ac, respectively. Performing the extraction in acetone or ethanol led to films with similar characteristics. Prolonging the NH_3 treatment induced cracks and delamination of the coatings. As-prepared and treated films were optically transparent and crack-free. Their thickness could be varied from 200 to 1000 nm by adjusting the withdrawal rate and the sol dilution. The layer thickness at the edge of the samples was about 20% less than that at the center, gradually decreasing in a few millimeters from the edges.

2.2. Characterization Techniques. The structures of the as-prepared and treated coatings were studied by XRD, using the Cu Kα ray from a rotating anode. $\theta-2\theta$ diffractograms of films, deposited on glass substrates, were recorded with a conventional goniometer (acquisition time: 1 s/0.005° step). Diffracted patterns were recorded on image plates, in transmission mode, using a home-built diffractometer and two different geometries: a normal beam configuration and a grazing incident geometry for which the incident angle oscillated between −7° and +7° during acquisition. The distance between the film and the image plate was 700 mm, and the acquisition time was ranging from 2 to 10 h. For these latter analyses, 8-μm-thick silicon wafers were chosen as the substrate to reduce absorption and background effects. Details of the later experiment are described elsewhere.[20] In situ time-resolved SAXS experiments were performed at the Austrian high-flux SAXS beamline ELETTRA, Trieste, Italy. A dip coater has been specifically designed to fit the SAXS beamline; usually, the substrate is dipped in the container filled with the sol and then withdrawn at a constant rate. A modified version of the machine was built to move the container and to keep fixed in position the substrate. Experiments were performed on films deposited on the same 8-μm-thick silicon substrates, with an incident angle of 2° between the beam and the film surface. The evolution of the structure was followed during the first 5 min after deposition by recording the 2D diffraction patterns every second on a CCD camera. For each sample, a pattern was recorded on an image plate 10 min after deposition. Micrographs of the cross section of selected calcined films were obtained with a transmission electron microscope (TEM) JEOL 100 CX II apparatus. Coatings deposited on Si substrates were diamond-cut by microtomy and deposited on a carbon-coated copper grid.

Ellipsometry measurements were carried out with a variable angle spectroscopic ellipsometer (Woollam VASE instrument). Optical properties were deduced by fitting the obtained ellipsometric ψ and Δ optical quantities, measured at 10-nm intervals, between 400 and 1400 nm, for 53°, 56°, and 59° incidence angles. The models used for fitting consisted of a glass or silicon substrate with a porous SiO_2 film on top. The thickness and the refractive index (n) of the top layer were the only fitted parameters. The refractive index was varied by assuming a certain volume of voids in silica (using a Bruggeman effective medium approximation with a depolarization of 1/3). It should be noted that, within certain boundaries, the effect of varying the pore volume is fully correlated to varying the depolarization factor (which is related to the pore geometry). In the case of uniaxial anisotropy, the refractive index was split into an in-plan and a normal component. Average values of n are reported in this paper. The amounts of C, Si, and O per surface unit in the films were determined by Rutherford backscattering (RBS), using a 2.5 MV Van de Graaf accelerator and a normal incident beam of 2 MeV $^4He^+$ ions. The energy of the backscattered He^+ was analyzed using a silicon surface barrier detector, positioned at 10° from the incident beam. The spectra are given as normalized yield (i.e., counts at the detector per mC He dose) versus energy. Spectra were quantified by simulations, using a stack of layers with varying amounts of the relevant elements.

Surface area, porosity, and minimum pore size were estimated from N_2 adsorption/desorption analysis, performed directly on the S_{350} calcined films. The measurement was performed on 47 dip-coated glass substrates (24 × 50 × 0.4 mm). These coated plates, corresponding to a total weight of 22 ± 3 mg of mesoporous material, were sealed in a glass cell adapted for the BET analysis. A Micromeritics ASAP 2000 apparatus was used to record the nitrogen adsorption−desorption isotherm at 77 K on the full range of relative P/P_0 pressures. Details of this method adapted to thin films have been reported recently by Ayral et al.[19]

3. Results

3.1. 1D XRD in ($\theta-2\theta$) Scan Mode. In a first experiment, films were prepared from sols containing

(19) Ayral, A.; El Mansouri, A.; Vieira, M. P.; Pilon, C. *J. Mater. Sci. Lett.* **1998**, *17*, 883.

(20) Klotz, M.; Albouy, P. A.; Ayral, A.; Ménager, C.; Grosso, D.; Van der Lee, A.; Cabuil, V.; Guizard, C. *Chem. Mater.* **2000**, *12*, 1721.

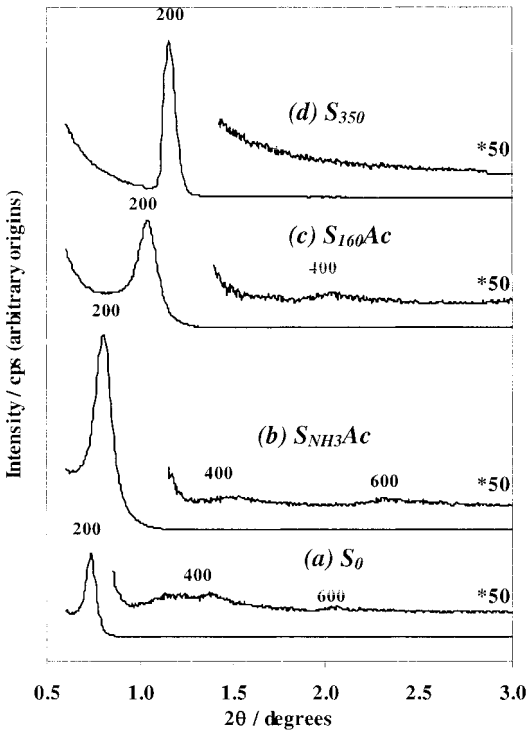

Figure 1. 1D XRD diffraction diagrams, obtained in $\theta-2\theta$ mode, for the as-prepared and treated coatings deposited on glass plates. The main peaks were indexed (200) from a centered rectangular lattice. The maximum intensities were respectively 35 K for the as-prepared S_0 film (a), 95 K for the $S_{NH3}Ac$ films (b), 45 K for the $S_{160}Ac$ films (c), and 85 K for the S_{350} films (d).

the same amounts of TEOS, HCl, EtOH, and H_2O, but varying amounts of F127. Only as-prepared coatings prepared with F127 compositions ranging from 3.3 to 6.1 wt % show organization by XRD. In this paper, only coatings prepared with 5.5 wt % of surfactant (reference sol) will be discussed as they exhibit the highest peak intensities and the largest interplanar distances. Films deposited from solutions containing higher concentrations of F127 either are not transparent or undergo a F127 segregation over long periods of aging (e.g., >12 h).

Figure 1 shows the XRD diagrams of the as-prepared (a) and treated (b−d) coatings deposited at 2.5 mm s^{-1} on glass collected with a $\theta-2\theta$ goniometer. In each case, an intense and narrow peak is recorded at low angles that corresponds to an interplanar spacing of 135 Å for S_0, 121 Å for $S_{NH_3}Ac$, 89 Å for $S_{160}Ac$, and 79 Å for S_{350}. Each main peak intensity exceeds 4×10^4 cps with the line width at half-height less than 0.1°. With the exception of S_{350}, harmonics of the main peak with low intensities are observed. The decrease of the observed distance applies in the direction normal to the surface with the largest contraction obtained after calcination at 350 °C. Less contraction was found with the two-step $S_{160}Ac$ treatment, but the increase in the main peak width in addition to its lower intensity is a sign of a slight alteration of the structure. Indeed, the two-step $S_{NH3}Ac$ method should be considered as the best treatment in terms of shrinkage minimization.

3.2. 2D XRD in Transmission Mode. The results presented in Figure 1 make difficult the description of the 3D structure of the films. To obtain a better characterization, the films were analyzed by 2D XRD in transmission. The *a* lattice parameters in the rectangular cell are deduced from the following results for each treatment and are reported in Table 1. The patterns obtained with as-prepared and $S_{NH3}Ac$ treated films are presented in Figure 2, with two different X-ray incidence angles with respect to the film surface. When the beam is normal to the surface, the diffraction patterns show a single well-defined intense ring. The corresponding interplanar spacing is as follows: 148 Å for S_0 and 140 Å for $S_{NH3}Ac$. It remains almost constant with the treatment because it corresponds to planes that are perpendicular to the film surface and for which the shrinkage is minimum.

At grazing incidence, the patterns now show ellipses. They are attributed to planes that have at least one direction collinear to the beam; the small axes of the ellipses correspond to the distances measured in the previous geometry with the beam normal to the surface. The interspacing distances deduced from the longer axes of the ellipses vary as follows: 128 Å for S_0 and 109 Å for $S_{NH3}Ac$. They correspond to the same diffraction planes as those responsible for the main peak observed in Figure 1 with a *d* spacing maximum discrepancy of

Table 1. Rectangular Cell Parameters (*a*) Deduced from XRD, Refractive Indices (*n*) Obtained by Ellipsometry at 550 nm, Layer Thickness (*h*) Obtained by Ellipsometry, and Porosity (*P*) Deduced Either from the Refractive Index (*n*) or by Comparing Thickness (*H*) with *h* ($P = 100(h - H)/h$)[a]

				shrinkage/%		porosity (*P*)/%	
treatment	*a*/Å	*n*	*h*/nm	from *d*(200)	from *h*	from *n*	from RBS
S_0[b]	256	1.47 ± 0.01	612 ± 30	0	0		
S_{350}	146	1.30 ± 0.03	383 ± 20	43	36	35 ± 5	56 ± 3[c]
$S_{160}Ac$	188	1.26 ± 0.02	410 ± 20	26	31	41 ± 4	60 ± 2
$S_{NH_3}Ac$	218	1.22 ± 0.04	500 ± 15	15	14	49 ± 6	66 ± 2

[a] Average extents of shrinkage induced by the treatments were deduced from the thickness contraction (using $(h_0 - h)/h_0$ with $h_0 = 612 \pm 30$) and from the XRD measurement of $d(200)$ in $\theta-2\theta$ mode. *H* and h_0 were constant for all coatings: $H = 167 \pm 8$ nm and $h_0 = 612 \pm 30$ nm. [b] The *p*6*m* hexagonal phase is indexed with rectangular symmetry, $b = a_0$ (hexagonal cell) and $a = \sqrt{3}a_0$. *a* is collinear and *b* perpendicular to the substrate. [c] From BET, a value of 63 ± 3% was obtained.

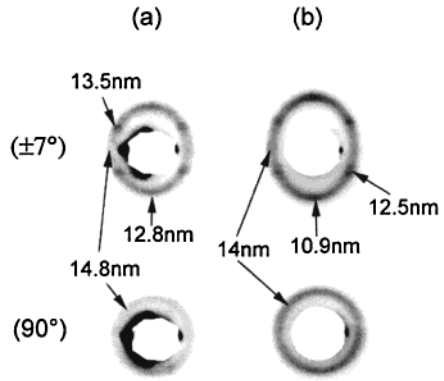

Figure 2. 2D XRD diffraction patterns obtained at grazing incidence (top) and at a 90° incidence angle (bottom). These were recorded for a sample/image plate distance of 700 mm and are displayed here with an enlarged scale for better clarity (as-prepared S_0 film (a); $S_{NH3}Ac$ films (b). The *d* values reported on the patterns correspond to the interplanar spacings calculated from the distances measured between the center of the ellipses and the diffraction spots indicated by the arrows.

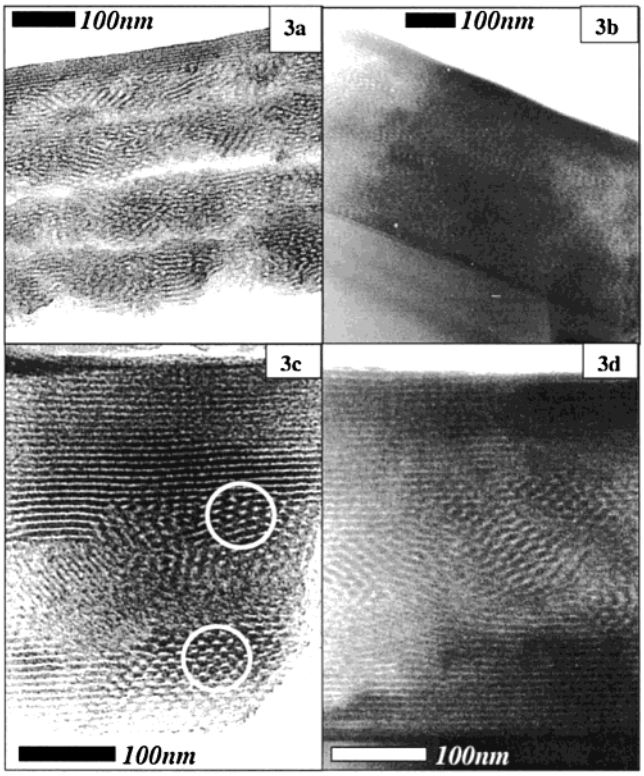

Figure 3. TEM micrographs of cross-sectioned film produced with the reference sol (a) and (b) and the reference sol diluted twice with ethanol (c) and (d).

10% between both techniques. The XRD patterns are consistent with a 2D hexagonal lattice (*p*6*m*) for the as-prepared films and a 2D centered rectangular lattice for the treated film. The rectangular cell parameters are $a = 256$ Å and $b = 148$ Å for the as-prepared film and $a = 218$ Å and $b = 140$ Å for the $S_{NH3}Ac$ film. The structure of the as-prepared film can also be described as 2D hexagonal with $a_H = b_H = {}^1/_2{*}256{*}(3/4)^{1/2} = 148$ Å. The ellipsoidal continuous diffraction is attributed to domains that have random orientations with respect to the film surface. Its particular ellipsoidal shape is due to a different degree of shrinkage induced by the unidirectional contraction depending on the orientation. This observation has been well described and explained in a recent paper.[20] The diffraction spots positioned on the ellipse are due to well-aligned domains that have their *c* axis preferentially aligned with the surface plan. They correspond to *d* values of 135 Å for the as-prepared film and 125 Å for the $S_{NH3}Ac$ one and are consistent with (110) plans in the centered rectangular structure. The fact that the diffracted rings recorded in normal beam geometry (90°) are continuous and of similar intensity all over the ring suggests that no preferred orientation of the channels was induced by the substrate withdrawal direction in the surface plan.

3.3. TEM. TEM analysis was performed on cross sections of S_{350} samples. Figure 3a,b displays images of a film deposited from the reference sol containing EtOH/TEOS = 20 while Figure 3c,d corresponds to film deposited from the same reference sol but diluted to EtOH/TEOS = 40. They both exhibit two different types of phase located at different depths in the film profile. A well-aligned phase can be seen at the air/film and film/substrate interfaces and a second randomly oriented phase is located between the well-aligned phases within the film center. These pictures confirm the hypothesis of the presence of two phases, suggested by the 2D XRD patterns of Figure 2. In Figure 3c, one can clearly see that both types of phases are formed of elongated domains composed of pores arranged in a 2D centered rectangular array (white circles).

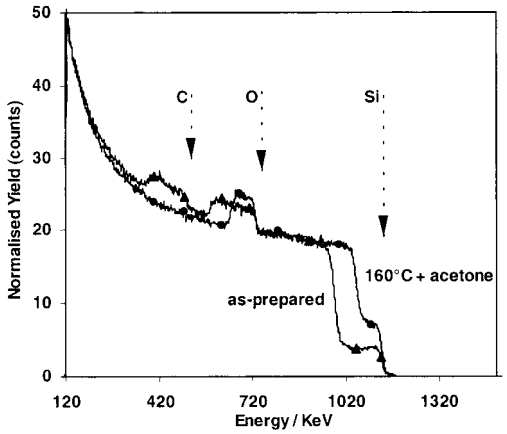

Figure 4. Atom content profiles obtained by RBS for the as-prepared (▲) and the $S_{160}Ac$ (●) films.

3.4. RBS. The RBS depth profile analysis shows that the distribution of atoms is uniform for both as-prepared and treated samples (Figure 4), indicating that no composition gradient exists in the layers and that the distribution of organic domains in S_0 was homogeneous within the coatings. The amounts of Si per surface unit obtained by simulation for S_0, $S_{160}Ac$, S_{350}, and $S_{NH3}Ac$ films ranged from 360 to 380 $\times$ 10^{15} atoms cm^{-2}. The as-prepared coating consists of a layer containing Si, O, and C, while the treated films only contain Si and O, implying that the organic phase was effectively removed after each treatment. Taking into account the initial amounts of O and C contained in F127 and the fact that the silicate network is not expected to be fully condensed, the surface density of O for the untreated coating by RBS was found to be much smaller than what is expected. The difference may be induced by the He^+ bombardment: He^+ ions can transfer enough energy to break covalent bonds, leading to decomposition, especially of organic materials. The amount of C and O are therefore not discussed in more detail for the as-prepared sample. For $S_{160}Ac$, S_{350}, and $S_{NH3}Ac$ films, the O/Si composition ratios were found to be between 2.08 and 1.97 and are attributed to the extent of condensation, as the organic phase has been completely removed. From the Si content and the estimated density of the silica walls (2.3 g cm^{-3}), one can deduce the theoretical thickness (*H*) of the dense SiO_2 layer expected if the studied films were nonporous. *H* should be constant for each sample and was calculated to be 167 $\pm$ 8 nm.

3.5. Ellipsometry. Refractive indices (*n*) and thickness (*h*) of as-prepared and treated films were deduced from ellipsometry and are given in Table 1. The porosity was obtained from the refractive indices, assuming an effective medium approximation with spherical voids in the silica matrix. Note that a different geometry and orientation of the pores may lead to values of the pore volume that differ by about 5%. The thickness nonuniformity for the measurement area was less than 5%. The thickness of as-prepared films was measured to be

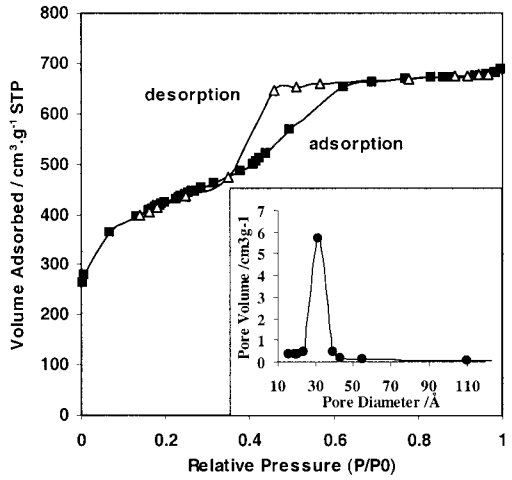

Figure 5. N_2-BET adsorption−desorption isotherm and BJH pore size distribution obtained with S_{350} films.

612 ± 30 nm. They exhibit a high refractive index (i.e., 1.47 at 550 nm) close to that of dense SiO_2, suggesting that the pores are filled with the organic phase. After treatment, both the refractive index and the film thickness decrease due to the combined effect of surfactant removal and network unidirectional shrinkage. For S_{160}-Ac and S_{350} films, the measured data could not be described correctly, assuming an isotropic coating. For these latter, ψ and Δ plots were best fitted, assuming a uniaxial anisotropy or a refractive index gradient. Anisotropy is consistent with the orientation of the cylinders with respect to the surface. The presence of denser phases at both film interfaces is consistent with a gradient in the refractive index**.** The lowest averaged refractive index of 1.22, which gives 49% porosity (Table 1), was obtained for the S_{NH3}Ac treatment, which confirms the lowest contraction induced by such two-step methods. S_{350} and S_{160}Ac films exhibit respective refractive indices of 1.30 (about 35% porosity) and 1.26 (about 41% porosity).

3.6. N_2-Adsorption/Desorption Investigation. Figure 5 shows the N_2 adsorption/desorption isotherm of type IV obtained for S_{350} films. The large hysteresis loop is characteristic of capillary condensation that takes place in mesoporous materials containing cylindrical pores with bottlenecks. The comparison of the BET surface area (1470 ± 200 $m^2\ g^{-1}$) and of the BJH adsorption cumulative surface area of pores (800 ± 100 $m^2\ g^{-1}$) suggests the presence of a significant amount of micropores. The adsorption cumulative pore volume was deduced to be 0.75 ± 0.1 $cm^3\ g^{-1}$. This corresponds to a porosity of 63 ± 3%, when taking 2.3 g cm^{-3} as the density of the silica matrix. The BJH adsorption evaluation of pore diameter gives a relatively large distribution of 32 ± 15 Å, due to various degrees of pore contraction during treatment.

3.7. In Situ Time-Resolved SAXS. The in situ SAXS investigation allows one to follow the structural formation of the mesostructured hybrid films during dip coating. 2D X-ray diffraction patterns are given in Figure 6 at different times after deposition for different sol compositions. Three cases are presented. Figure 6a represents the structural formation of a film deposited from the reference sol and used for the previous investigations. Figure 6b,c corresponds to films obtained

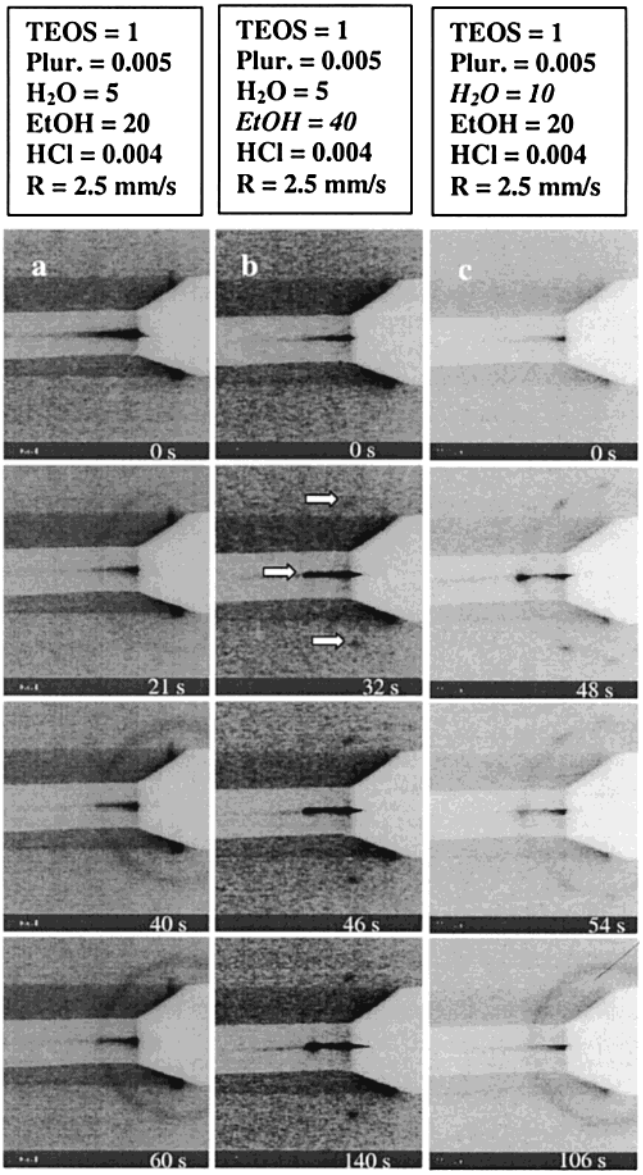

Figure 6. Structural evolution of film observed by in situ SAXS analysis during dip coating.

from sols containing a higher amount of ethanol or a higher amount of water, respectively. For the reference system, one can clearly see that there is no organization in the first 20 s and that a diffraction ring appears after this period of time. The corresponding distance corresponds to that found in the XRD pattern in the absence of contraction. This diffraction ring is due to the organization of the cylindrical micelles into domains that are not well-aligned with the surface of the film, but with the *c* axis randomly oriented, as suggested by the continuity of the diffraction ring.[20] The pattern does not change up to the end of the acquisition (3 min). A diffraction pattern was then recorded 10 min later on an image plate (Figure 7a). It shows the diffraction ring accompanied this time by diffraction spots corresponding to well-aligned hexagonal domains. This indicates that the interface mesophase was formed at a later stage in the film formation process, between 3 and 10 min after deposition.

The system containing a higher content in alcohol shows the straight appearance of the diffraction spots after 32 s (white arrows), but no diffraction ring.

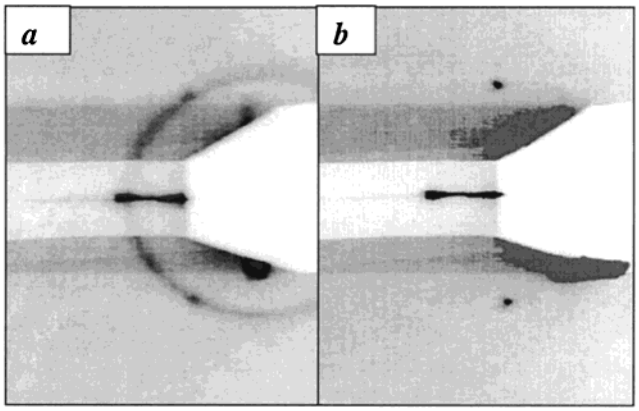

Figure 7. 2D diffraction patterns obtained 10 min after deposition and corresponding to films deposited from the reference sol (a) and from the reference sol twice diluted with ethanol (b).

Increasing the ethanol content leads to a longer drying time and to a thinner film.[21] In this particular case, only the well-aligned phase is progressively formed without passing by the formation of disoriented domains. The 2D diffraction pattern in Figure 7b was taken 10 min after deposition and confirms the absence of the diffraction ring. A similar observation was made during the deposition of the reference sol at a lower withdrawal rate (results not shown). Decreasing the deposition rate or increasing the alcohol content lead to thinner films, suggesting that the formation of both types of phases can be related to the film thickness. Moreover, the formation of a well-aligned 2D hexagonal structure is favored for thinner films.

A more aqueous sol produces films that do not present any diffraction spots corresponding to the well-aligned 2D hexagonal organization, even 10 min after deposition (Figure 6c). After 106 s the pattern is only composed of the diffraction ring, suggesting that the whole film is formed of disoriented domains. However, one can clearly remark the formation of an intermediate phase between 45 and 55 s characterized by diffraction spots. They could not be properly indexed but they confirm that an intermediate phase only exists for a few seconds when depositing a water-rich solution (i.e., $H_2O/TEOS \geq 10$).

4. Discussion

4.1. Film Formation Mechanism. The phase diagrams of the Pluronic F127[22,23] show that a primitive cubic structure arising from the arrangement of spherical micelles is the only mesostructure observed in pure water. In the presence of water and alcohol, cylindrical micelles can also be formed and both cubic and 2D hexagonal mesophases can be observed, depending on the concentration. In the more alcoholic conditions used for this work, the 2D hexagonal structure was the only one observed on the fully dried films. It is however possible to prepare cubic *Pm*3*n*, 2D hexagonal *p*6*m*, and 3D hexagonal $P6_3/mmc$ silica mesostructures from TEOS and F127 in ethanol, as recently reported.[10−12] During deposition of the solution by dip coating, the preferential evaporation of ethanol and then water at the air/film interface induces gradients of concentrations in F127, silica species, and HCl.[16,17] Above the critical micelle concentration (CMC), micelles start to form and the condensation of the silica species becomes more and more favored as the pH decreases and the water content increases. The initial solution is isotropic and the concentration from which the first mesostructure forms is reached at the interface after 20 s of solvent evaporation with our reference sol (5.5 wt % F127). This organization further expends toward the film/substrate interface due to the progressive increase in concentration driven by the evaporation. This first phase is composed of bunches of cylindrical micelles that organize into 2D hexagonal arrays. They can be called domains. Early in the film formation, these domains have random orientations as confirmed by the presence of the diffraction ring only. Later in the drying process, the diffraction pattern shows the presence of diffraction peaks that prove the realignment of the domain *c* axis with the film surface. Moreover, the 2D hexagonal structure is observed only at the film interfaces and forms between 3 and 10 min after the deposition when the film can be considered dry.

We can thus suppose the following mechanism for film prepared from the reference sol: spherical, and then cylindrical, micelles first form in an ethanol-rich environment upon evaporation. A few tens of seconds after deposition, cylindrical micelles self-organize into randomly oriented 2D hexagonal domains. After 3 min when the evaporation is considered to be done, the silica phase is still flexible enough to allow for the domains that are close to the interfaces to realign with the interfaces. This interfacial alignment drives the reorganization to propagate from the interfaces to the center of the film. In parallel, the silica matrix undergoes further condensation as a result of H^+ and water enrichment first followed by drying and gelling, leading to the progressive rigidification of the inorganic network. Both realignment and condensation are in competition. At a certain time along this process, the structure of the film just freezes out as the silica network is too rigid to undergo further reorganization. If the film is thin enough, well-aligned phases may gather at the film center. On the other hand, if the film is too thick or the initial sol is relatively too highly condensed, a randomly orientated phase of domains remains at the film center between both well-aligned interfacial phases. Figure 3c shows a film where most of the domains had time to realign with the interfaces before rigidification of the silica walls. The competition between the self-assembly alignment and the condensation leads to the latter structures observed in most of the 2D hexagonal mesostructured films.

We have seen that an intermediate structure is observed between 45 and 55 s when $H_2O/TEOS \geq 10$. In this particular case, the global water content is higher than that in the previous case. After deposition, ethanol departs first from the layer before water. There is a short period of time where the system is rich in water[17] and where the composition $EtOH/H_2O/F127$ favors the formation of such an intermediate structure.

(21) Brinker, C. J.; Frye, G. C.; Hurd, A. J.; Ashley, C. S. *Thin Solid Films* **1991**, *201*, 97.
(22) Wanka, G.; Hoffmann, H.; Ulbricht, W. *Macromolecules* **1994**, *27*, 4145.
(23) Holmqvist, P.; Alexandridis, P.; Lindman, B. *Langmuir* **1997**, *13*, 2471.

Further water evaporation induces the transition of this phase into the 2D hexagonal domains observed and described previously. This phenomenon confirms that the formation of a 2D hexagonal mesophase is promoted by a more alcoholic medium, as reported in the phase diagrams.[22,23] For this water-rich solution, the diffraction pattern does not show diffraction peaks 10 min after deposition. The lack of realignment may be due to a higher degree of condensation of the inorganic species induced by the high water content.

Similar experiments have been performed using cetyltrimethylammonium bromide surfactant (CTAB) as the structuring agent.[24] Similar influences of the withdrawal rate and condensation degree have been observed, except that the final film structure is reached earlier than with F127 (i.e., around 30 s with CTAB against around a few min with F127). The kinetics of self-assembly is thus found to be slower with neutral surfactants as block copolymers. The silica−F127 self-assembly process under acidic conditions was described as a $S^0H^+X^-I^+$ process,[10] where S^0 represents the nonionic surfactant, H^+ and X^- are assigned to dissociated HCl, and I^+ is the positively charged silica matrix. In the present case, most of the silica species are nonprotonated due to the low HCl content. The process is then better described as S^0I^0, suggesting that the self-assembly process and the formation of the mesostructure occur via nonelectrostatic weak interactions. These interactions, weaker than those with ionic surfactants, are only due to the more hydrophilic character of the poly(ethylene oxide) chains. This may explain the low initial degree of organization of the micelles early in the process and their slow kinetics of alignment.

4.2. The Film Structure. We have deduced from XRD and TEM data that as-prepared coatings have a 2D hexagonal structure while treated coatings exhibit a 2D centered rectangular structure. By setting the ellipse's longer axes to correspond to the *a* parameter and the smaller one to the *b* parameter of a centered rectangular lattice, one observes that *b* did not significantly change, while *a* is reduced during treatment (Table 1). In the particular case of a 2D hexagonal *p*6*m* structure, the lattice parameters must verify the following relation: $a = b\sqrt{3}$. For the as-prepared coating, this relation is verified as $a = 2d(200) = 256$ Å and $b = d(010) = 148$ Å. The reduction of *a* is the reason for the transformation of a 2D hexagonal structure into a 2D centered rectangular structure. This implies that the rectangular structure arises from the unidirectional shrinkage of the initial hexagonally arranged film during treatment. Actually, this is an approximation as the domains have various orientations and the distortions induced by the treatments have different intensities depending on the orientation with respect to the direction of the contraction. This phenomenon has been described in detail in a separate paper.[20] In these films, domains are preferentially aligned with the substrate surface plane, making swirling patterns. Such a feature has already been shown by Lu et al.[6] with mesoporous silica films produced with ionic CTAB, where single-pore channels were arranged into a wormlike structure. In comparison, our F127/SiO_2 films showed whole-organized domains, spinning, twisting, and curving with respect to the *c* axis of the channel direction. The reason the diffraction peaks are located on the diffraction ring is that the formation of the interfacial phases are due to the reorganization of domains rather than micelles initially arranged in a wormlike structure. The realignment of such disoriented micelles would lead to smaller characteristic distances, while domains exhibit the same lattice parameter before and after realignment with the surface.

4.3. Physical Properties. Values for the refractive index *n* and the layer thickness *h* are reported in Table 1 for the various applied treatments. The porosity (*P*) as deduced from *n*, and also calculated from *h* and *H* with the relation $P = 100(h - H)/h$, are also reported. The discrepancy found between the porosity obtained by both methods can be explained in terms of an inappropriate relation between the refractive index and the porosity. Materials that have the same porosity but different morphology and orientation of pores with respect to the incident beam direction will exhibit different refractive indices as a result of the different dielectric responses. As in the present cases the pore channels are for most of the domains preferentially aligned with the surface plane, the refractive indices are higher than what would be measured for isotropic materials of similar porosity. Thus, the porosity deduced from *n* is underestimated and values given by the adsorption/desorption isotherms of gas or by the combined ellipsometry-derived layer thickness and the RBS-derived surface amount of SiO_2 are closer to the real porosity. In addition, the hydrophilic character of the silica walls promotes the adsorption of water within the pores, further reducing the refractive indices measured by ellipsometry. However, the changes in the refractive index are easy to determine and can be regarded as consistent with relative variations in porosity.

During film formation, the hydrophilic PEO chains may penetrate the silica matrix, as suggested by Melosh et al.[11,12] Once the copolymer is eliminated and the inorganic network condensed, the porous structure must contain micropores as well as mesopores due to the penetration of the PEO chains into the inorganic walls. In addition, diblocks and monoblocks are often present when using commercial copolymer triblocks. Such isolated PEO chains may be found anywhere in the matrix, accentuating the content in micropores after elimination. This accounts for the high surface area and porosity observed by BET (i.e., 800 $m^2\ g^{-1}$ and 63%, respectively).

4.4. Influence of Treatment. We have shown that the organized structure survives after the various treatments used to remove the surfactant. A unidirectional shrinkage occurs in the films, leading to 2D centered rectangular structures. Table 1 also shows the comparison of the refractive index *n* and the percentage of shrinkage deduced from the thickness contraction $100(h_0 - h)/h_0$ or from the *d*(200) XRD-measured contractions. Each sample exhibits a reduction of thickness after treatment, induced by the unidirectional shrinkage in the direction normal to the surface of the substrate. The extent of the contraction depends on the type of treatment applied and varies between 15 and 43%. Taking into account that the surfactant is com-

(24) Grosso, D.; Albouy, P. A.; Amenitsh, H.; Balkenende, A. R.; Babonneau, F. *Mater. Res. Soc. Symp. Proc.* **2000**, *628*, in press.

pletely removed by the treatment, the porosity should decrease (increasing the refractive index) with the extent of contraction for similar films. This is also evident from the changes in the refractive index. The $S_{NH3}Ac$ treatment induces less contraction (15%) and therefore leads to the highest porosity and the lowest refractive index ($n = 1.22$). The progressive thermal treatment from 160 to 350 °C simultaneously induces the thermal decomposition of the copolymer surfactant, recorded by TGA to take place between 160 and 250 °C on similarly prepared silica/F127 composite xerogel and further condensation of the network via dehydration. On the other hand, the two-step treatments involve the condensation of the network while the surfactant micelles remain within the pores, withstanding the contraction induced by the condensation. The surfactant micelles can then be assimilated to supporting materials that allow for the inorganic network to slowly stiffen, before being removed. The elimination of the surfactant at low temperature prevents the shrinkage induced by a too high and sudden high-temperature treatment. The shrinkages are therefore lower than those observed after treatment at 350 °C.

5. Conclusion

The present paper has described synthetic approaches for preparing highly organized mesoporous thin silica films at low temperature (<160 °C), using block copolymers as structuring agents. The resulting complex nanostructures of the films have been accurately characterized using a combination of TEM observations made on film cross sections and 1D and 2D XRD measurements. Under our experimental conditions, as-prepared films present a 2D hexagonal geometry. Indeed, TEM and XRD investigations show that these films are formed of two types of phases. A phase with randomly oriented domains of organized pore channels is found at the film center, while at both interfaces (air/film and film/substrate) the channels are well aligned with the surface. To get better insights into the mechanisms of formation of such mesostructured films, in situ time-resolved SAXS experiments were performed for the first time. They allow us to follow in real time the development of the film organization and to suggest a possible mechanism for the formation of such mesostrucures. First, cylindrical micelles self-organize in the liquid film into randomly oriented 2D hexagonal domains. Then the domains, which are close to the interfaces (air/film and substrate/film), tend to align parallel to the surfaces. This alignment progresses toward the film center. The extent of alignment will be governed by the condensation rate of the silica network, whose stiffening at a certain point will prevent further alignment of the domains. Consequently, depending on the experimental conditions (composition of the starting solution, withdrawal rate), the ratio between randomly oriented domains and well-aligned domains will vary.

Several treatments have been developed to remove the surfactant under moderate temperature conditions. They are accompanied by a unidirectional shrinkage of the 2D hexagonal initial structure, which transforms into a centered rectangular structure. The amplitude of the shrinkage depends on the applied treatment. A two-step method, involving precondensation of the network by NH_3 and subsequent removal of the copolymer by extraction in hot acetone, seems the most appropriate to keep a high degree of ordering and to obtain high porosity (around 65%). It is important to point out that the determination of the pore volume of these films is delicate: usually, the porosity is estimated from the refractive index measured from ellipsometry. But in such anisotropic materials, which may also contain an appreciable amount of adsorbed water, the pore volume seems to be underestimated. Combination of ellipsometry and RBS measurements, or N_2-adsorption−desorption measurements, appear to be more reliable techniques.

These films are attractive as antireflective and low dielectric coatings. For such applications, other parameters than porosity have to be taken into account, e.g., the water content of the layer (affecting the dielectric properties) and the mechanical properties. But thorough insight into the layer structure will always be a prerequisite for more application-oriented studies, and this paper demonstrates that techniques are available to reach a detailed description of the film mesostructure.

Acknowledgment. The authors would like to acknowledge the financial support from Philips and the help received from the following researchers: Y. Tamminga and H. Snijders (Philips, Eindhoven) for the RBS analyses, M. Lavergne (LRS, UPMC, Paris) for the TEM analyses, and A. El Mansouri (LMPM, ENSCM, Montpellier) for the N_2-BET investigation. The EC funding for ELETTRA synchrotron investigation was greatly appreciated. We would also like to thank BASF for providing the Pluronic F127 surfactant.

CM001225B